International Journal of Scientific Engineering and Applied Science (IJSEAS) – Volume-8, Issue-5, May 2022
ISSN: 2395-3470
www.ijseas.com

Experimental Evaluation of an Ammonia-Water Absorption Refrigeration System Cooled By Air

P. Soto, I. Román, D. Hernández and W. Rivera*

Instituto de Energías Renovables, Universidad Nacional Autónoma de México, Temixco, Morelos, México.

*Corresponding author: E-mail address: wrgf@ier.unam.mx

ABSTRACT

The assessment of a novel absorption refrigeration system cooled by air using ammonia-water is reported. Flat plate heat exchangers are used in the evaporator, the generator, and the economizer, while finned-tubes are used in the condenser and the absorber. A fan is used to remove the heat delivered by the condenser and the absorber. The system's performance has been analyzed as a function of diverse parameters such as generator temperature, condenser temperature, fan power, solution concentrations, and mass flow rates. The system showed to be very sensitive to the variation of almost all the parameters. The cooling powers varied from 0.1 to 3.8 kW, while the performance's coefficients varied from 0.05 to 0.53, obtaining evaporator temperatures as low as – 10.5 °C.

Keywords: absorption cooling system, ammonia-water, air-cooled

1. Introduction

The International Energy Agency (IEA), reported energy supply is unsustainable from any point of view [1]. On the other hand, the International Refrigeration Institute reported that refrigeration and air conditioning systems consume approximately 15% of the world's total electricity production [2]. Likewise, it has been reported that 45% of total residential energy consumption is due to air conditioning systems [3]. Because absorption cooling systems can be operated with industrial waste heat or renewable energies, they can be used to reduce the electricity consumed around the world.

Although there have been many studies related with the development of prototypes of absorption cooling systems operating with water/lithium bromide (H_2O/LiBr) [4, 5, 6], ammonia/water (NH_3-H_2O) [7, 8, 9, 10, 11, 12], and even with alternative mixtures as the ammonia-lithium nitrate (NH_3-$LiNO_3$) mixture [13, 14, 15, 16, 17, 18, 19, 20], all of them

are water-cooled systems, and just a few ones mentioned below have been designed to remove the heat produced in the condenser and the absorber by using air.

Rivera et al. [21] reported the experimental assessment of a cooling system for ice production using a compound parabolic solar collector as a generator-absorber operating with NH_3-$LiNO_3$. The evaporator is a thermally insulated box. Inside the box, a coil is attached to the trays where the water is deposited to produce the ice. The absorber is cooled by air flowing in natural convection. The minimum evaporator temperature achieved by the system was −11 °C. The heat source temperatures varied between 75 and 110 °C. The maximum amount of ice produced was 8 kg/day. Moreno-Quintanar et al. [22] carried out the experimental assessment of the same system but using NH_3-$LiNO_3$-H_2O. The authors reported that the solar coefficients of performance (COP) increased by up to 24% compared to the values published by Rivera et al. [21] with NH_3-$LiNO_3$.

Du et al. [23] evaluated a two-stage absorption air conditioning system cooled by air operating with the NH_3-H_2O, powered by solar energy. The system operated with three levels of pressure with one refrigerant circuit and two solution circuits. To remove the heat produced in the absorber and condenser consisted of vertical finned tubes, the system used two-phase motors to drive two fans. The remaining components were shell and tube heat exchangers. The COPs of the system varied from 0.13 to 0.29, achieving the lowest evaporator temperature of -5.8 °C.

Lizarte et al. [24] compared the performance of a commercial absorption cooling system indirectly air-cooled, with a prototype of an air-cooled absorption cooling system. Both systems using H_2O-LiBr, with a nominal cooling capacity of 4.5 kW. The prototype consisted of an adiabatic absorber, two solution pumps, a regenerator, a finned-tube heat exchanger, and a fan. The condensation temperature ranged between 28 and 37 °C, with a generation temperature of 105 °C. The results showed that the commercial system cooled water at 18 °C, while the prototype achieved a temperature of 16 °C. The COP of the commercial system was 0.55 compared to 0.62 obtained with the prototype.

Jawahar and Saravanan [25] experimentally evaluated an absorption cooling system cooled by air using the NH_3-H_2O mixture. This system was modified by incorporating GAX in the high and low-pressure zones. The absorber and condenser were finned-tubes heat exchangers

while the rest of the components were shell and tube heat exchangers. The system was capable of producing a cooling power of 9.5 kW, with a COP of 0.61 at a generation temperature of 120 °C and 2 °C in the evaporator.

Zamora et al. [26, 27] reported the assessment of two air conditioning systems using the NH_3-$LiNO_3$ mixture. One of the system was fully cooled by water, while the other prototype used air to cool the condenser. The maximum cooling capacity of both prototypes was 12 kW producing chilled water at a temperature of 15 °C.

Aprile et al. [28] developed a double-lift absorption air conditioning system cooled by air operating with the NH_3-H_2O mixture driven by hot water. The system was able to produce chilled water at 7 °C. The generator was a vertical shell-and-tube falling-film heat exchanger. The evaporator was a shell-and-tube vertical flow countercurrent heat exchanger, while the condenser and absorber were steel tubes coils with vertical aluminum fins. The authors reported the system performance as a function of the generator temperature, the ambient temperature, and the fan power. The cooling capacity was 2.5 kW with a COP of 0.3 at an air temperature of 30 °C and hot water driving temperatures between 80 °C and 90 °C.

Cai et al. [29] compared the performance of a single-effect absorption refrigeration cycle cooled by air operating with the NH_3-$LiNO_3$ and ammonia-sodium thiocyanate (NH_3-NaSCN) mixtures. The measured COP for the NH_3–NaSCN varied from 0.20 to 0.35, while with the NH_3–$LiNO_3$ mixture varied from 0.15 to 0.29. The lowest evaporation temperature achieved by the system using NH_3–$LiNO_3$ was -13.1 °C, while with the NH_3–NaSCN mixture was -7.5 °C. For both mixtures, the cooling capacity was around 600 W.

Goyal et al. [30] experimentally evaluated a prototype of an absorption cooling system operating with the NH_3-H_2O mixture. The system was operated by using the exhaust gases from a diesel engine. The absorber and condenser were finned tubes heat exchangers using a fan to circulate the air through them. The remaining components were packaged in a compact microchannel structure. The systems' cooling power varied from 1.91 kW to 2.54 kW, while the COP varied from 0.41 to 0.55 at ambient temperatures between 29.7 and 44.2 °C.

Soto and Rivera [31] reported the results of a single-stage absorption cooling system cooled by air using NH_3-LiNO. The prototype uses compact heat exchangers acting as a generator,

an evaporator and a heat exchanger, and finned tubes in the remaining components. The system operated at heat source temperatures vary from 80 °C and 100 °C, while condenser temperatures varied from 20 °C to 32 °C. The maximum external cooling load was 3.4 kW, while the maximum COP was 0.33. The lowest evaporator temperature was 2.6 °C.

From the literature, it can be observed that almost all the developed systems use water to remove the heat produced in the absorber or condenser, and just a few of them are entirely air-cooled. From the air-cooled prototypes, it was found that some of them operated with H_2O-LiBr, others with NH_3–$LiNO_3$, and just four of them were developed using the NH_3-H_2O mixture. From these four systems, the one developed by Du et al. [23] is a two-stage system developed for air conditioning using finned-tubes in the condenser and absorber and shell of tube heat exchangers in the rest of the components. The authors report COP values both did not perform a parametric analysis of the system. The one developed by Goyal et al. [30] uses finned-tubes in the absorber and condenser, a shell and tube heat exchanger in the desorber, and microchannels heat exchangers in the evaporator, in the refrigerant pre-cooler, and the solution heat exchanger. The authors analyzed each of the components' performance and the variation of the cooling duty and COP as a function of the ambient temperature, but they did not perform a parametric study of the system as a function of any other variable. The prototype developed by Jawahar and Saravanan [25] incorporated the GAX processes in the high and low-pressure zones, requiring temperatures higher than 120 °C to run the system, and it was built with-finned tubes in the absorber and condenser, and shell and tubes heat exchangers in the remaining components. They reported COP values, but they also do not perform a parametric study. Finally, the prototype developed by Aprile et al. [28] was a double-lift system designed to produce chilled water at 7 °C. The absorber and condenser were again built with finned tubes, and the generator and evaporator were shell and tube heat exchangers. The authors reported the cooling load and COP variation as a function of the fan power, and generator and air temperatures.

From the analysis of the prototypes developed using the NH_3-H_2O mixture, it is clear that none of them use compact plate heat exchangers in any of the components. Three of them are complex systems requiring temperatures higher than 120 °C to operate, and only in one of them, a parametric study was performed, but they did not use compact heat exchangers. Based in the bibliographic review, an air-cooled single-stage absorption cooling system was designed and built operating with the NH_3-H_2O mixture at the Instituto Energías Renovables

of the Universidad Nacional Autónoma de México. In a similar way to the previously developed air-cooled prototypes, in the actual system finned-tubes are used in the absorber and condenser, but instead of using shell and tube heat exchangers in the remaining components, flat plate heat exchangers are used. The system is designed to operate at generator temperatures between 95 °C and 115 °C. A parametric analysis is performed to analyze the cooling capacity and the COP of the system as a function of the fan power, generator temperature, air temperature, solution concentrations, and system mass flow rates.

2. System description

2.1 Main components

The systems' main components are three compact heat exchangers (CHE) acting as a generator, evaporator and an economizer, three finned-tubes coils acting as the condenser, rectifier, and absorber, an axial fan, and two small tanks used to storage the solution.

The specifications of the heat exchangers the finned-tubes acting as the condenser and absorber have been reported by Soto and Rivera [31]. The rectifier is a finned-tube heat exchanger similar to the condenser and absorber but with a total length of 45 cm. A piston pump is used to pump the solution from the absorber to the generator. One tank of 1.65 liters capacity is used to separate the refrigerant from the solution at the exit of the generator, and a second tank of the same capacity is installed at the exit of the absorber to store the NH_3-H_2O solution. An axial fan is installed to control and circulate the air through the system cooling the absorber and condenser. An auxiliary system integrated by an electric resistance, a hot water storage tank, and a pump is used to carry out the experimental assessment under controlled conditions. The specifications of the pump, the fan, and the auxiliary system have also been reported by Soto and Rivera [31]. Figure. 1 shows a general sketch of the prototype developed.

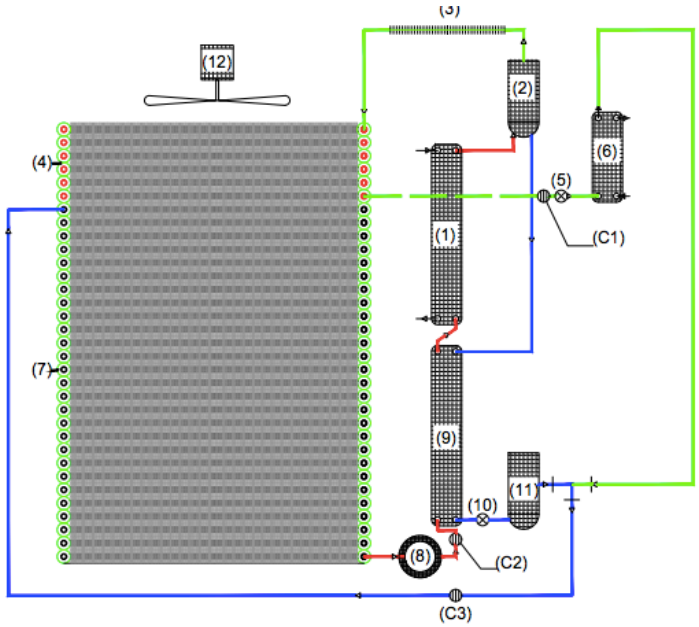

1. Generator
2. High pressure buffer
3. Rectifier
4. Condenser
5. Expansion valve
6. Evaporator
7. Absorber
8. Solution Pump
9. Economizer
10. Restrictor valve
11. Low pressure buffer
12. Fan

Diluted solution stream
Concentrated solution stream
Refrigerant stream

C1: Refrigerant Coriolis Sensor
C2: Concentrated Solution Coriolis Sensor
C3: Diluted Solution Coriolis Sensor

Figure 1. Schematic diagram of the system.

2.2 Operation of the system

As can be observed from Fig. 1, hot water is supplied to the generator (1) to heat the concentrated ammonia-water mixture flowing through the component. Then, the heated solution goes to the separation tank (2) where the ammonia with some amount of water in a vapor phase flowing toward the top of the tank passes to the rectifier (x). Heat is removed in the rectified condensing almost all the water in the vapor, which returns to the generator, while the ammonia is almost pure passes to the condenser (3). In this component, the ammonia vapor is condensed by the heat removed from the air flowing through it. The weak solution coming out of the bottom of the separation tank passes to the economizer (8), then through the valve (9), and then enters the low-pressure tank (10). Then, the solution coming out of the low-pressure-tank passes to the absorber (6). On the other hand, the ammonia coming out of the condenser is expanded in the valve reducing its temperature (4). Then, the

ammonia enters the evaporator producing the cooling effect. After this, the vapor ammonia enters the absorber, where it is absorbed by the weak ammonia solution coming from the generator. The heat produced as a result of the exothermic reaction during the absorption process is removed by the air passing through the absorber's finned-tubes. The strong solution leaving the absorber is pumped (7) to the generator passing first through the economizer. In the economizer, the strong solution is preheated by the weak solution coming from the generator. Finally, the preheated solution enters the generator, repeating the cycle again. An axial fan (11) is used to circulate the air through the finned-tubes banks of the absorber and condenser.

2.3 Data Acquisition

The developed prototype has been instrumented to measure temperatures, pressures, and mass flow rates. Soto and Rivera reported all the instrumentation specifications used in the experimental set up [31]. Figure 2 shows a schematic diagram of the systems pointing where the measurement instruments were placed, and Figure 3 shows the absorption cooling system fully developed and instrumented.

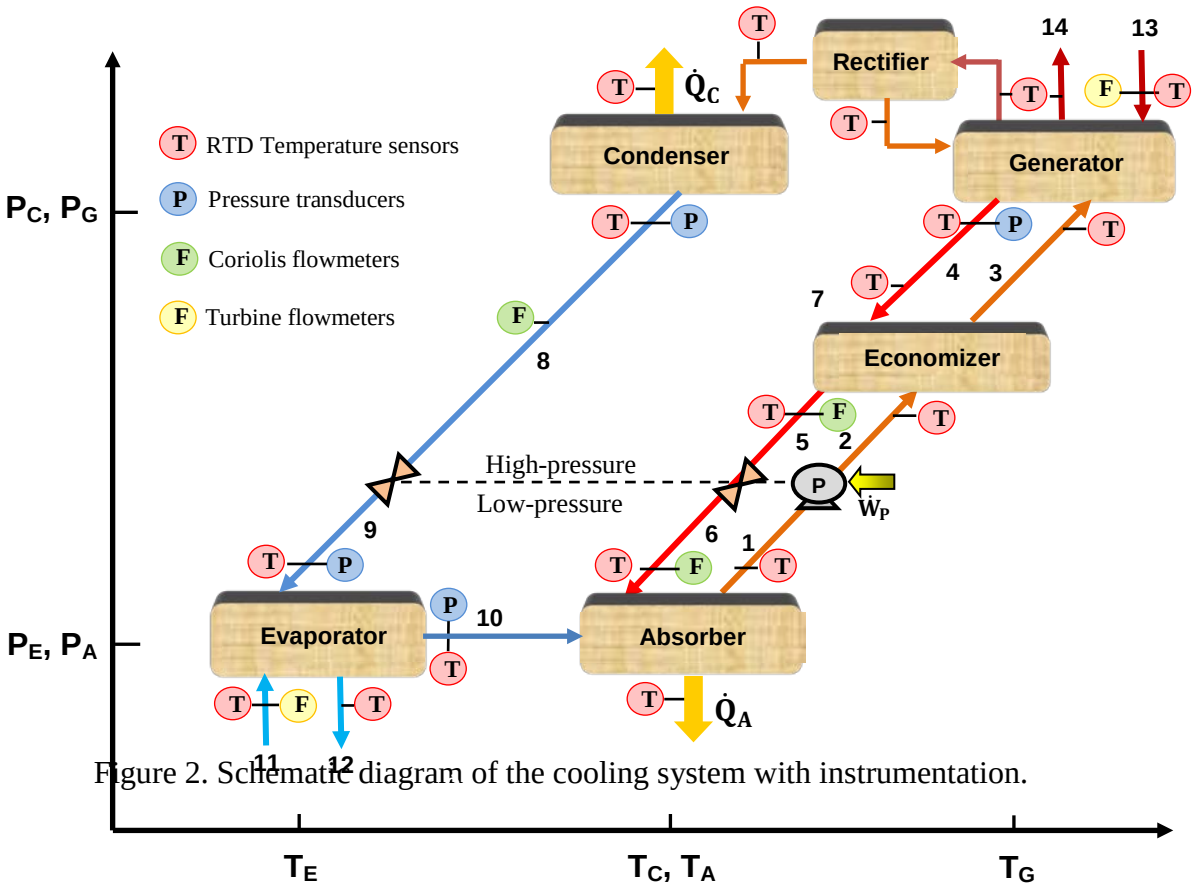

Figure 2. Schematic diagram of the cooling system with instrumentation.

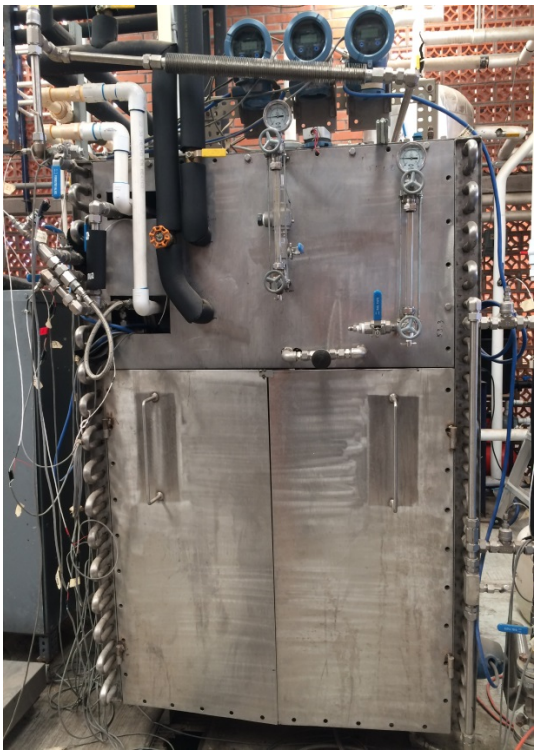

Figure 3. Absorption cooling system fully developed.

3. Main equations

The external coefficient of performance (COP_{ext}) can be calculated by the following equation:

$$COP_{ext} = \frac{\dot{Q}_{Eext}}{\dot{Q}_{Gext} + \dot{W}_{P-F}} \quad (1)$$

$\dot{Q}_{Eext}$ is the external cooling load produced by the system, $\dot{Q}_{Gext}$ is the external energy supplied to the generator, while $\dot{W}_{P-F}$ is the power supplied to pump and the fan. $\dot{Q}_{Eext}$ is calculated from Eq. (2), where $\dot{m}_{wi}$ is the mass flow rate of the water circulating through the evaporator, and h_{12} and h_{11} are the enthalpies of the water entering and leaving from the evaporator, respectively, according to Fig. 2.

$$\dot{Q}_{Eext} = \dot{m}_{wi}(h_{12} - h_{11}) \quad (2)$$

$\dot{Q}_{Gext}$ is calculated from the following equation:

$$\dot{Q}_{Gext} = \dot{m}_{hw}(h_{13} - h_{14}) \quad (3)$$

Where $\dot{m}_{hw}$ is the hot water mass flow rate circulating through the generator, and h_{13} and h_{14} are the enthalpies of the hot water entering and leaving from the generator.

$\dot{W}_{P-F}$ is calculated directly by measuring the voltage and current from the pump.

$$\dot{W}_{P-F} = V * I \quad (4)$$

Error propagation

Equation (5) and (6) were used for the error propagation according to the methodology proposed by Surendra [32].

$$u\{A + B\} = \sqrt{u\{A^2\} + u\{B^2\}} \quad (5)$$

$$\left(\frac{u\{A\ x\ B\}}{A\ x\ B}\right) = \left(\frac{u\{A\ /\ B\}}{A\ /\ B}\right) = \sqrt{\left(\frac{u\{A\}}{A}\right)^2 + \left(\frac{u\{B\}}{B}\right)^2} \quad (6)$$

4. Results

An analysis was realized to study the variation of the cooling power and the coefficients of performance as a function of the fan power, the generator temperature, the condenser temperature, the solution concentrations, and the system mass flow rates. The prototype operated in steady-state conditions for at least 30 minutes for every testing point.

4.1 Analysis of the variation of the generation and condenser temperatures on the system performance

To analyze the effect of the generation and condenser temperatures on the system performance, the generation temperature and the water to be cooled entering the evaporator remained constant while the condenser temperature varied along the experimental test run.

Subsequently, the generation temperature was changed and kept constant together with the water entering the evaporator, while the condensation temperature was varied again. The generator temperature varied from 95 °C to 115 °C in steps of 5 °C, and the cooling air temperatures in the range of 20 - 30 °C, in steps of 1 °C. The constant parameters during the tests are specified in each graph.

Figure 4 shows the variation of $\dot{Q}_{Eext}$ as a function of T_C. The maximum $\dot{Q}_{Eext}$ is 2.4 kW, while the minimum is about 0.1 kW. It is also shown that the maximum $\dot{Q}_{Eext}$ vales are achieved at higher generation temperatures, and the minimum cooling loads are obtained at low generation temperatures as in the case of 95 °C. This is because, at high generation temperatures, the generator's refrigerant increases, thus increasing $\dot{Q}_{Eext}$. Besides, $\dot{Q}_{Eext}$ decreases with the increment of T_C. This happened because the increment of T_C causes an increment of P_C and P_G, increasing the mixture's boiling point, thus reducing the refrigerant production. It can be seen that there are not values reported of the cooling power at condenser temperatures higher than of 28 °C and 26 °C at the generator temperatures of 105 °C and 110 °C, respectively. This happened since, during the experimentation, the day got cloudy, and the ambient temperature never rose up above those values.

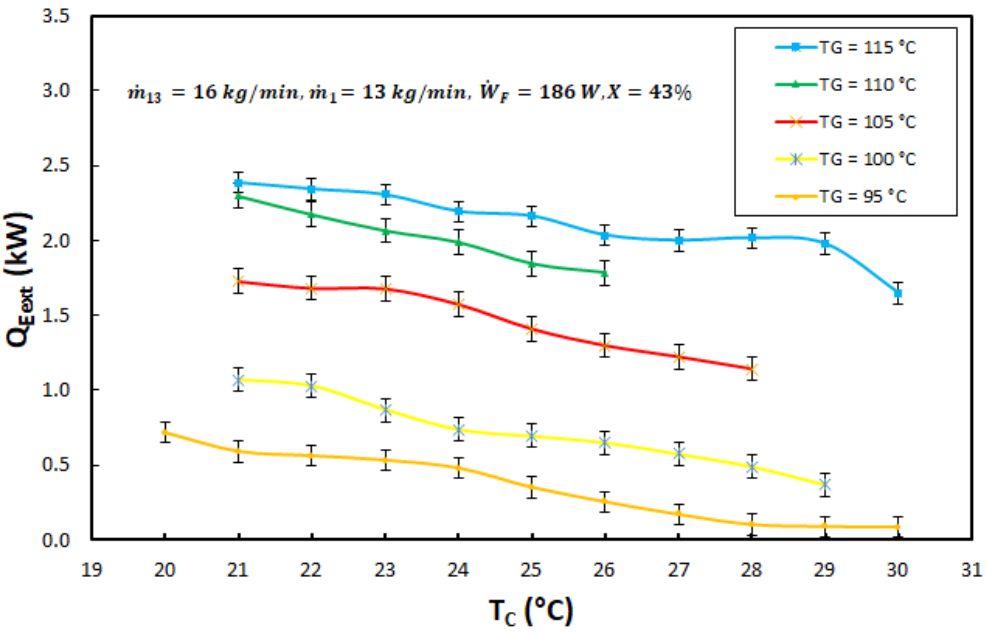

Fig. 4 $\dot{Q}_{Eext}$ against T_C for different T_G at X = 43%.

Figure 5 shows the COPext of the cooling system against T_C for different T_G values. It can be see that the COPext presents similar tendencies as a function of the condenser and generator temperatures than those reported in Fig. 4 for the $\dot{Q}_{Eext}$; that is, increases with the increment of T_G, and decreases with the increment of T_C for the same reasons explained in Fig. 4. This behavior was expected since, according to Eq. (1), the COPext is directly proportional to $\dot{Q}_{Eext}$. This figure also shows that the maximum COPext is 0.34 for a T_G = 115 °C and a T_C = 21 °C, at a solution concentration of 43%.

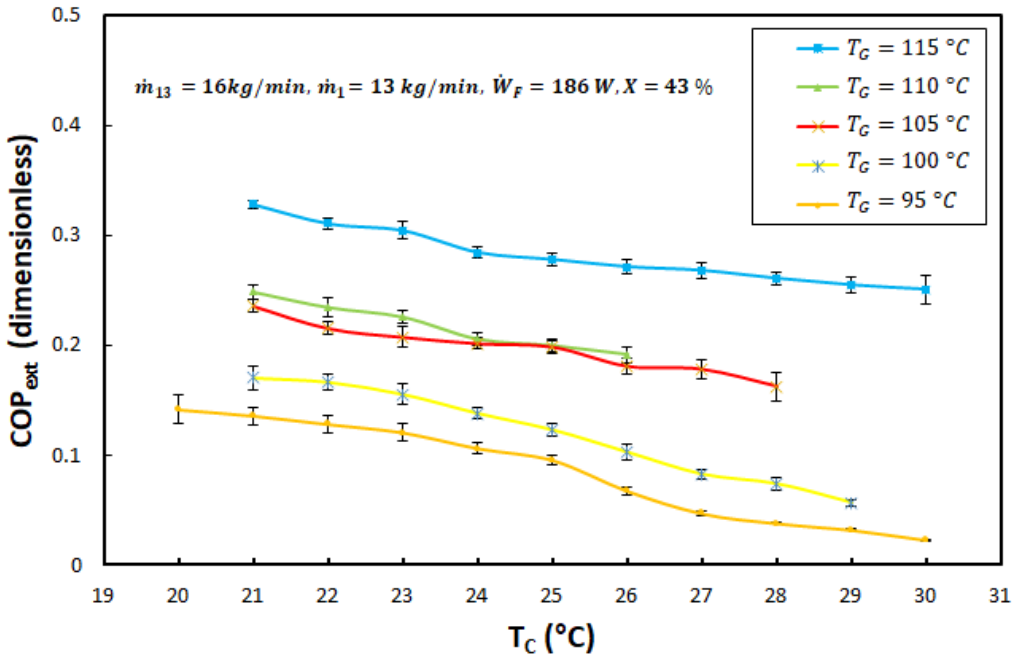

Fig. 5 COPext against T_C for different T_G at X = 43%.

Figure 6 shows the T_E's variation as a function of T_C for the same test runs showed in Figs. (4) and (5). It can be observed that T_E augments with the increment of T_C. This effect happens because the increment of T_C causes a pressure increase in the component, affecting the expansion process through the valve increasing T_E. Also, T_E significantly increases with the increment of T_G. This effect occurs because the increment of T_G causes an increment of the temperature in the entire solution circuit, including T_A, which also causes an increment in P_E, and therefore in T_E. It is shown that the minimum T_E is -9 °C, at a T_G = 95 °C and a T_C = 23 °C, while the maximum T_E is -2.2 °C, at a T_G = 115 °C and a T_C = 30 °C.

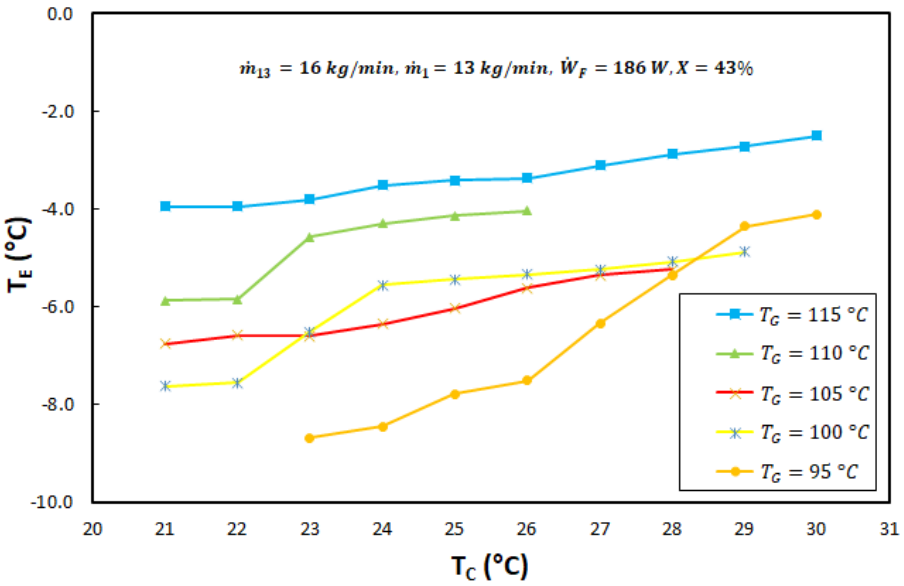

Fig. 6 Evaporator temperature against T_C for different T_G at X = 43%.

Figure 7 shows the $\dot{Q}_{Eext}$ as a T_C function for a solution concentration of X = 46%. It can be observed that $\dot{Q}_{Eext}$ decreases with the increment of T_C, and increases with the increment of T_G for the same reasons explained in Fig. 4. The maximum $\dot{Q}_{Eext}$ is 3.1 kW, at a T_G = 115 °C and a T_C = 20 °C, while the minimum is 0.4, at a T_G = 95 °C and a T_C = 28 °C. Comparing the cooling power values obtained in this plot at a solution concentration of 46%, with those reported in Fig. 4, for a solution concentration of 43%, it can be observed that the values obtained in this plot are higher.

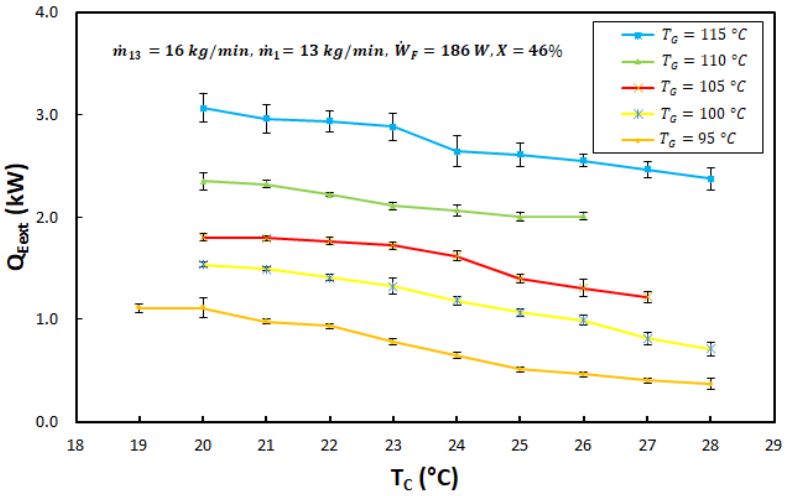

Fig. 7 $\dot{Q}_{Eext}$ against T_C for different T_G at X = 46%.

Figure 8 shows the COPext as a T_C function for different T_G at a solution concentration of 46%. It can be observed that the COPext presents similar tendencies as a function of T_C and T_G than those reported in Fig. 5. The maximum value of the COPext is 0.29 achieved at a T_G = 115°C and a T_C = 20 °C, while the minimum value is about 0.1, at a T_G = 95 °C, and a T_C = 28 °C.

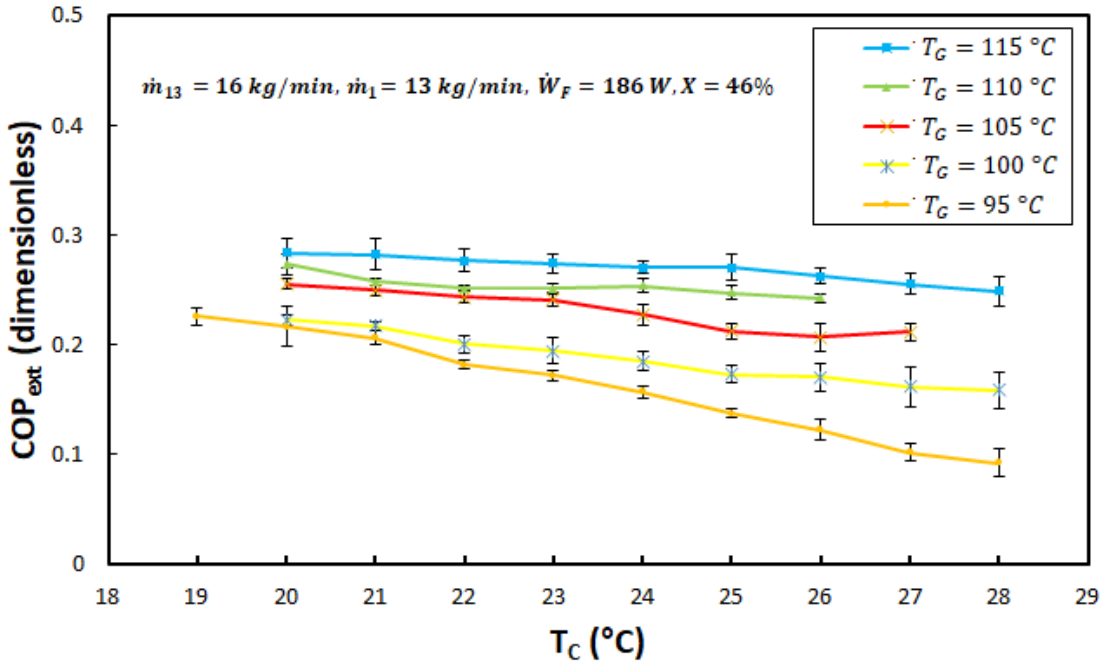

Fig. 8 COPext against T_C for different T_G at X = 46%.

Figure 9 shows T_E's variation as a function of T_C at a solution concentration of 46%. In this figure, it can be seen again that T_E lightly augments with the increment of T_C, and significantly with the increment of T_G, for the same reasons explained in Fig. 6. It is shown that the minimum T_E is -10.5 °C, at a T_G = 95 °C and a T_C = 19 °C, while the maximum T_E is 1 °C at a T_G = 115 °C and a T_C = 28 °C.

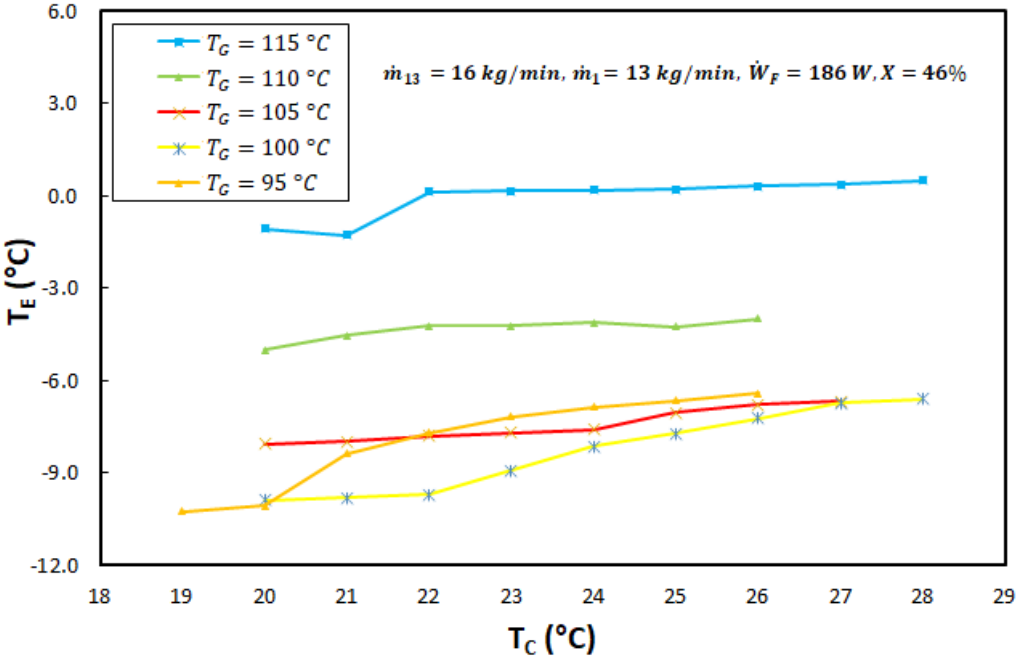

Fig. 9 Evaporator temperature against T_C for different T_G at X = 46%.

Figure 10 shows that $\dot{Q}_{Eext}$ decreases with the increment of T_C and increases with the increment of T_G, in a similar way, as shown previously in Figs. 4 and 7. The maximum $\dot{Q}_{Eext}$, in this case, is 3.6 kW, at a T_G = 115 °C and a T_C = 19 °C, while the minimum is 0.5, at a T_G = 95 °C and a T_C = 28 °C. Comparing the cooling power values obtained in this plot at a solution concentration of 49%, with those reported in Fig. 4 at an X = 43%, and in Fig. 7 at an X = 46%, it can be seen that the external cooling powers obtained at the solution concentration of 49% are approximately 14 % higher compared with the values obtained at X = 46 %, and around 33% higher regarding than those obtained at X = 43%. The $\dot{Q}_{Eext}$ increases with the increment of the solution concentration since at higher concentrations the ammonia produced in the generator will be higher, increasing with this the cooling power.

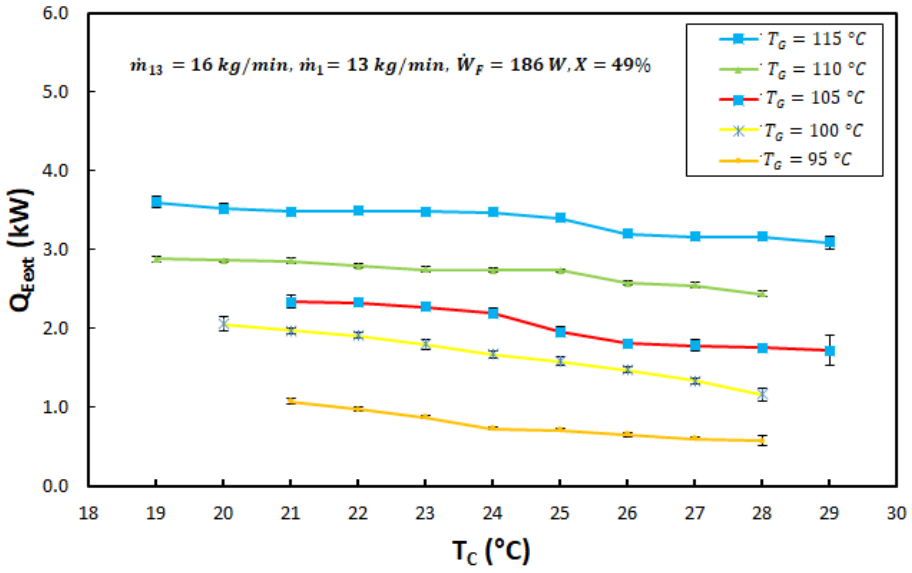

Fig. 10 $\dot{Q}_{Eext}$ against T_C for different T_G at X = 49%.

Figure 11 shows that the COPext slightly decreases with the increment of T_C and significantly increases with the increment of T_G. The maximum value of COPext is 0.36, obtained at a T_G = 115 °C, and a T_C = 19 °C, while the minimum value is about 0.1, at T_G = 95 °C, and a T_C = 28 °C. Comparing the COPext obtained in this figure with those obtained in Figs. 5 and 8, it can be observed that the COPext obtained at this concentration are higher than those obtained at lower solution concentrations. This occurs due to the increment of the cooling power at higher solution concentrations.

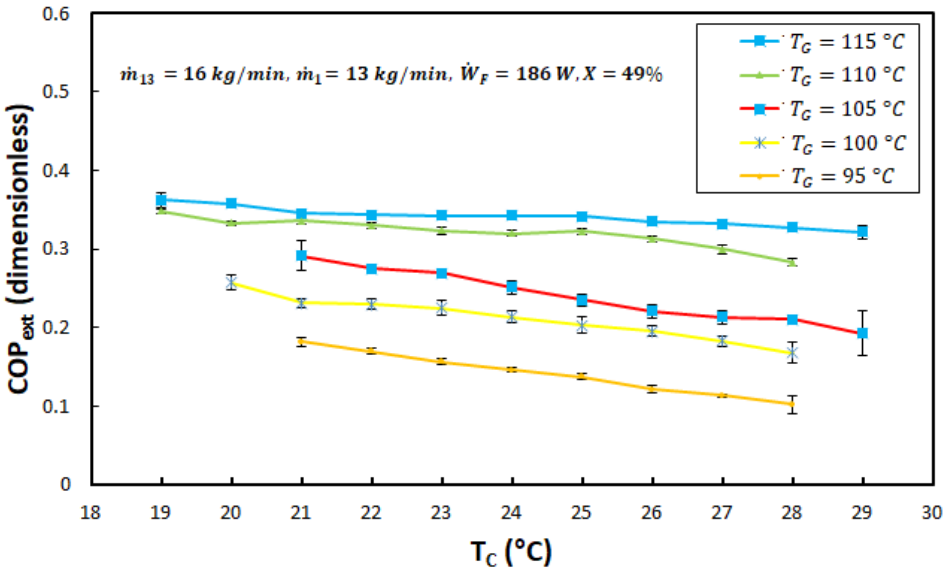

Fig. 11 COPext against T_C for different T_G at X = 49%.

Figure 12 shows T_E's variation as a function of T_C at a solution concentration of 49%. In this figure, it can be seen again the same tendencies of T_E with the increment of T_C and T_G showed in Figs. 6 and 9, but the evaporator temperatures continue to grow with the increase of the solution concentrations since now the minimum T_E obtained is -7.3 °C and the maximum is 2.3. The increase in T_E with respect to the concentration is because increasing the concentration increases the whole system's pressure, causing higher evaporation temperatures.

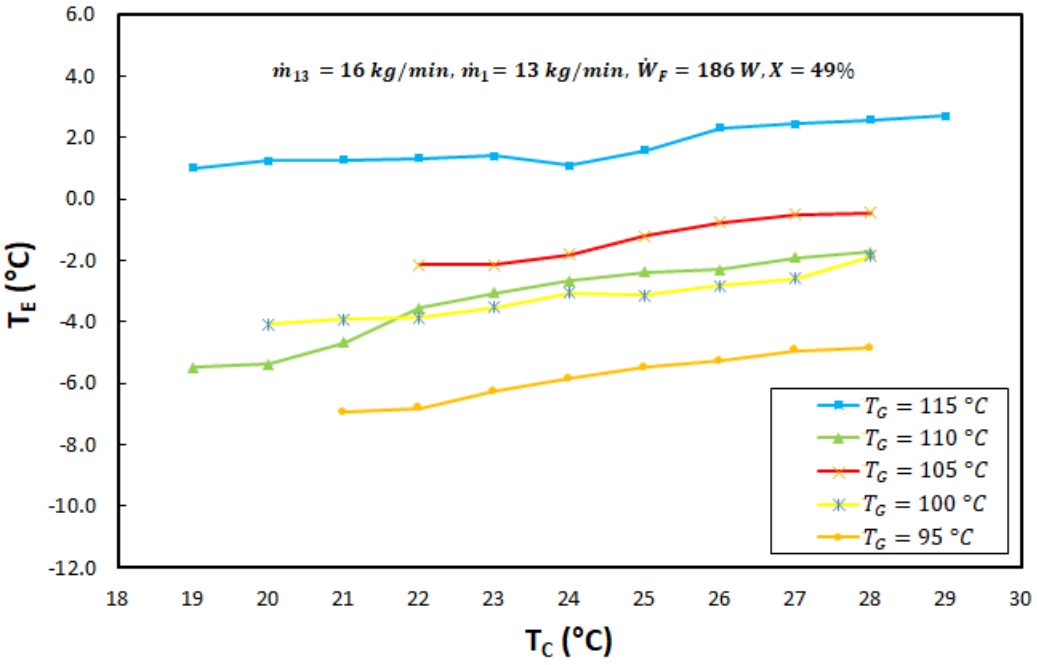

Fig. 12 Evaporator temperature against T_C for different T_G at X = 49%.

4.2 Analysis of the variation of the fan power on the system performance

To analyze the effect of the fan power on the system performance, the generation temperature and the water to be cooled entering the evaporator remained constant while the condenser temperature varied along the experimental test run, for a specific fan power. Subsequently, the fan power was changed, and the process was repeated again.

Figure 13 shows the $\dot{Q}_{Eext}$ against T_C for different fan powers at a solution concentration of 49%. It can be seen that the $\dot{Q}_{Eext}$ decreases with the increment of T_C, but increases with the increment of the fan power. This effect occurs since the increment of the fan power causes an

increase of the air velocity circulating through the absorber and condenser, improving these components' performance and the entire system.

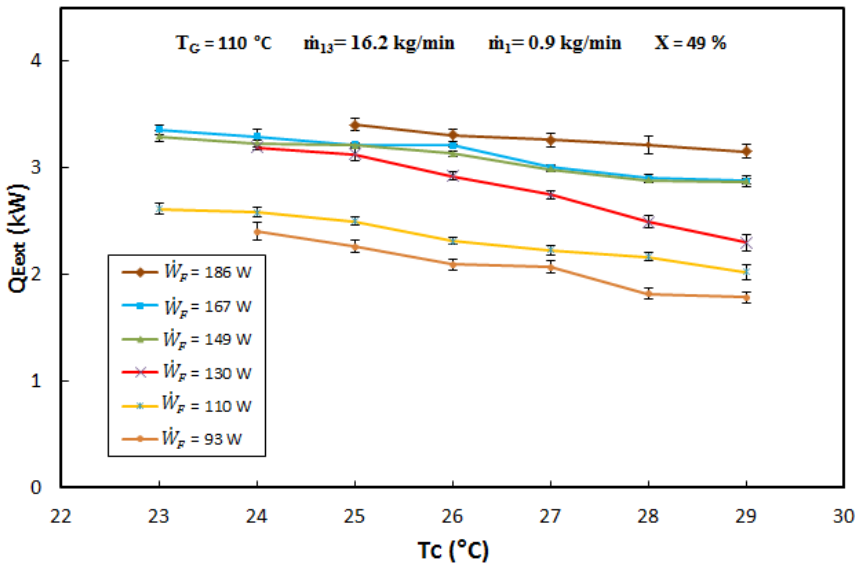

Fig. 13 $\dot{Q}_{Eext}$ against T_C for different $\dot{W}_F$.

In Figure 14 can be observed that the $\dot{Q}_{Eext}$ decreases with the increment of T_C, as it was seen in the previous section, but increases with the increment of the fan power. This effect occurs since the fan power increment caused an increase in the cooling power (as shown in Fig. 13), and therefore in the coefficient of performance.

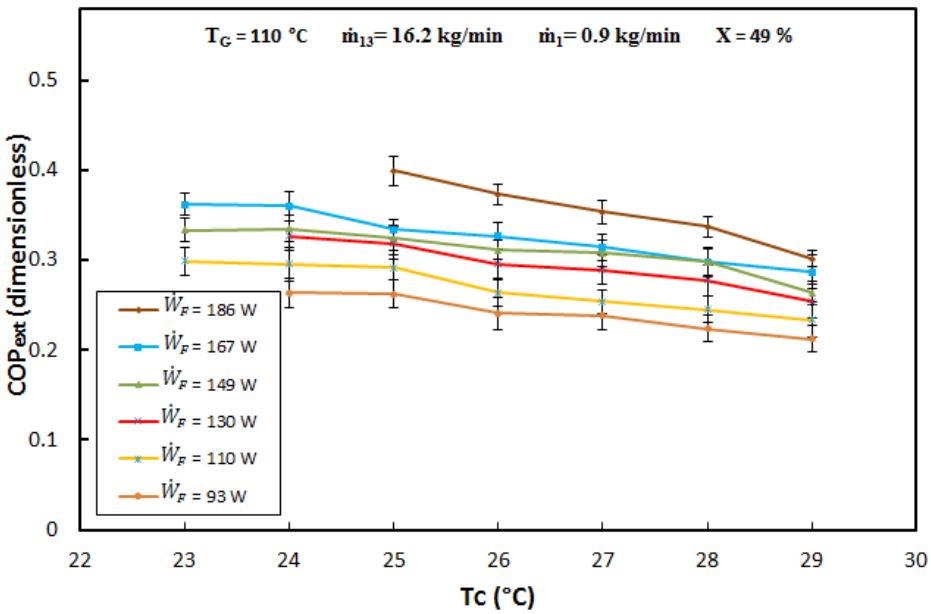

Fig. 14 COPext against T_C for different $\dot{W}_F$.

4.3 Analysis of the hot water mass flow rate on the system performance.

To analyze the effect of the hot water mass flow rate on the system performance, the generation temperature and the water to be cooled entering the evaporator remained constant while the condenser temperature varied along with the experimental test run for a specific hot water mass flow rate. Subsequently, the hot water flow was changed, and the process was repeated again. The parameters remaining constant are specified inside Figs. 15 and 16.

Figure 15 shows the $\dot{Q}_{Eext}$ as a function of T_C for different hot water mass flow rates at a solution concentration of 49%. It can be observed that $\dot{Q}_{Eext}$ slightly decreases with the increment of T_C for the reason explained in Fig. 4; however the $\dot{Q}_{Eext}$ considerably increases with the increment of the hot water mass flow rate supplied to the generator, since for the minimum value of $\dot{m}_{13}$ = 10 kg/min the $\dot{Q}_{Eext}$ varied from 2.2 kW to 1.9 kW, while for the maximum value of $\dot{m}_{13}$ = 18 kg/min the $\dot{Q}_{Eext}$ varied from 3.8 kW to 3.5, which is about 40% higher than the values obtained with the minimum flow. This effect occurs since the increment of the hot water circulating through the generator improves the heat transfer causing a higher production of refrigerant in the component, and therefore a higher amount of cooling power produced.

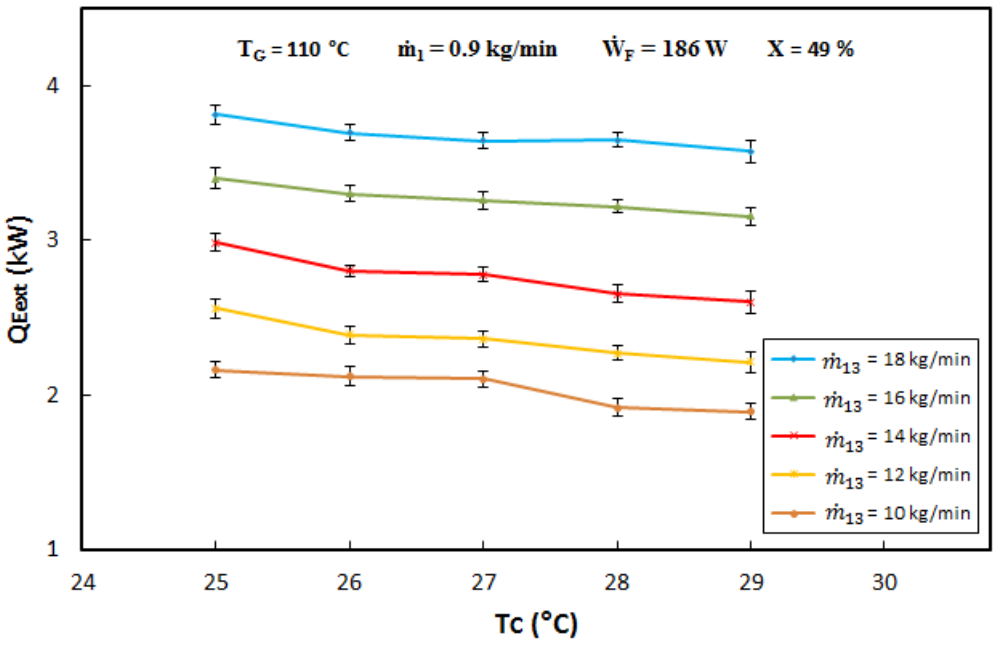

Fig. 15 $\dot{Q}_{Eext}$ against T_C for different heat water mass flow rates.

Figure 16 shows the COPext against T_C for different hot water mass flow rates at a solution concentration of 49%. It can be seen that the COP_{ext} decreases with the increment of T_C, and increases with the increment of the hot water mass flow rate. As it was expected, the COP_{ext} follows the same tendencies against T_C and $\dot{m}_{13}$ than those followed for the $\dot{Q}_{Eext}$ in Fig. 15. The minimum the COP_{ext} varied from 0.23 to 0.33 for a $\dot{m}_{13}$ = 10 kg/min, while the highest varied from 0.4 to 0.53 for a $\dot{m}_{13}$ = 18 kg/min.

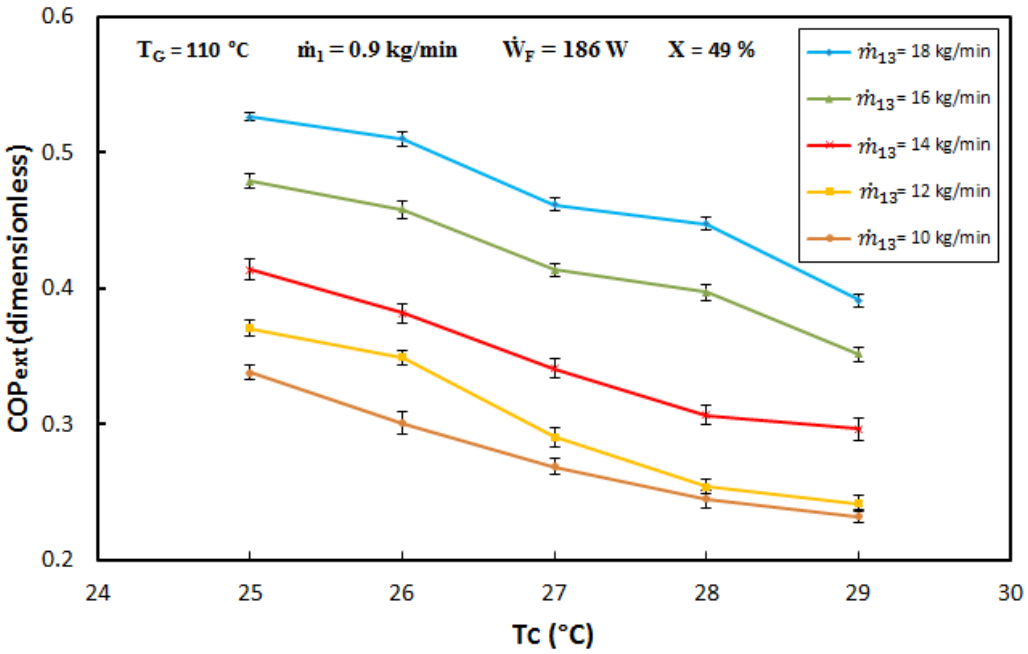

Fig. 16 COPext against T_C for different hot water mass flow rates.

4.3 Analysis of the solution mass flow rate on the system performance.

To analyze the effect of the solution mass flow rate going from the absorber to the generator on the system performance, the generation temperature and the water to be cooled entering to the evaporator were again kept constant, while the condenser temperature varied along the experimental test run, for a specific solution mass flow rate. Subsequently, the solution mass flow rate was changed, and the process was repeated again. The parameters remaining constant during the tests are specified inside Figs. 17 and 18.

Figure 17 shows the $\dot{Q}_{Eext}$ as a T_C function for different solution mass flow rates at a solution concentration of 49%. It can be seen that $\dot{Q}_{Eext}$ considerably increases with the increment of the solution mass flow rate going to the absorber to the generator, since for the minimum value of $\dot{m}_1$ = 0.48 kg/min, the $\dot{Q}_{Eext}$ varied from 1.6 kW to 2.1 kW, while for the maximum value of $\dot{m}_1$ = 1.23 kg/min the $\dot{Q}_{Eext}$ varied from 3.3 kW to 3.6, which is about 42% higher than the values obtained with the minimum flow. This effect occurs since the increment of the solution mass flow rate circulating through the generator, the economizer, and the absorber improves the heat transfer in these components, and therefore the system performance.

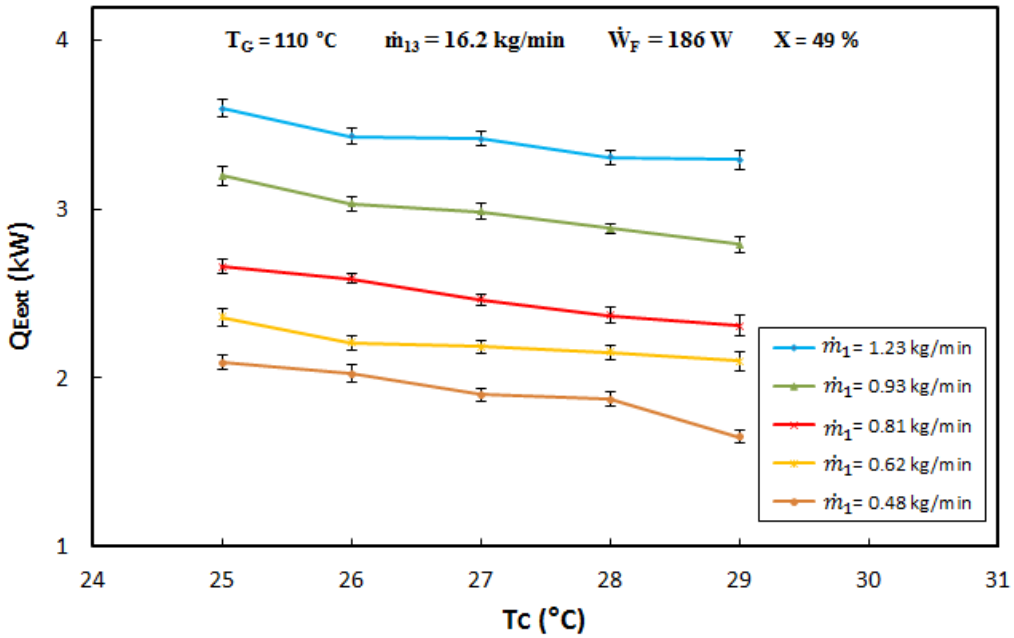

Fig. 17 $\dot{Q}_{Eext}$ against T_C for different solution mass flow rates.

In Fig. 18 it can be seen that the COP_{ext} decreases with the increment of T_C, and considerably increases with the increment of the solution mass flow rate. For the minimum flow of 0.48 kg/min, the COP_{ext} varied from 0.26 to 0.33, while for the maximum flow the COP_{ext} varied from 0.26 to 0.33 for a $\dot{m}_{13}$ = 10 kg/min, while the highest varied from 0.46 to 0.56 showing that the solution mass flow rate is a relevant parameter to improve the system performance.

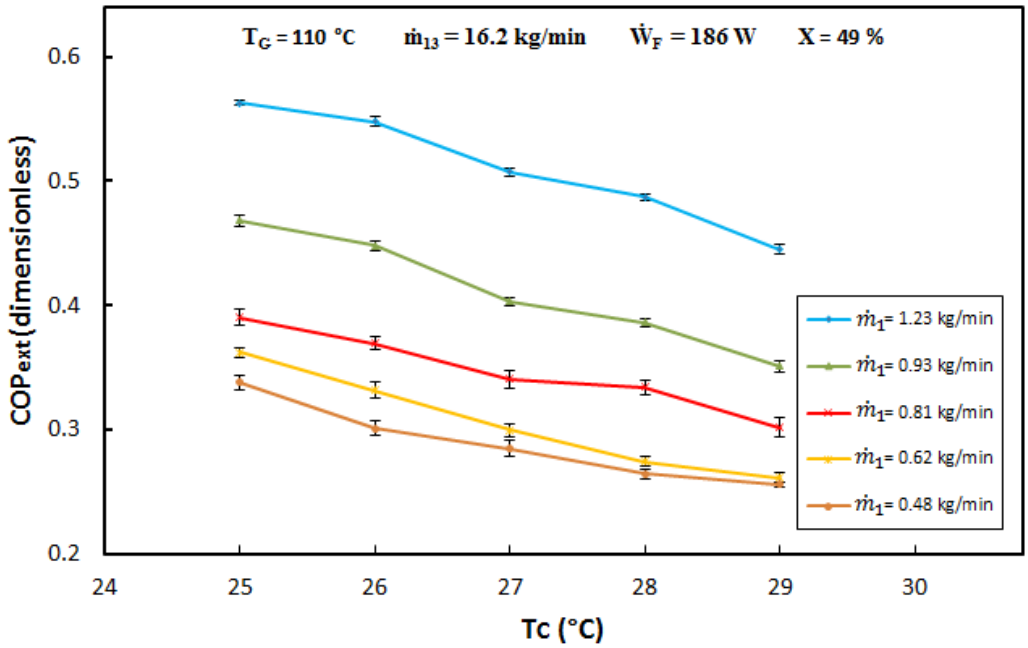

Fig. 18 COPext against T_C for different solution mass flow rates.

5. Conclusions

From the study, it can be concluded that at low solution concentration values, the system performance strongly decreases with the increase of the condenser temperature and significantly increases with the increment of the generator temperature; however, at high solution concentrations, the cooling power and coefficient of performance slightly decrease with the increment of the condenser temperature, and the variation with the generation temperature is still significant. The cooling power and the coefficients of performance increase with the increment of the solution concentration; however, at high solution concentrations, the evaporation temperatures were not so low. The analysis also showed that the system performance considerably improved with the fan power increment, and the hot water and solution mass flow rates. The $\dot{Q}_{Eext}$ varied between 0.1 kW and 3.8 kW, while the *COPext* varied between 0.05 and 0.53. The lowest cooling temperature obtained was -10.5 °C. The results showed that the system could be exclusively air-cooled, not requiring the use of a cooling tower.

Acknowledgments

The authors thank the *Fondo de Sustentabilidad Energética Secretaría de Energía-Consejo Nacional de Ciencia y Tecnología*, through the proyect *CeMIE-So P09*, for the economic support provided. Also, P. Soto is thankful for the scholarship provided by the Consejo Nacional de Ciencia y Tecnología.

Nomenclature

COP	coefficient of performance (-)
h	specific enthalpy (kJ/kg)
I	electrical current (amp)
$\dot{m}$	mass flow rate (kg/s)
P	pressure (bars)
$\dot{Q}$	thermal power (kW)
T	temperature (°C)
V	voltage (watts)
$\dot{W}$	power (kW)
X	ammonia concentration (%)

Subscripts

A	absorber
C	condenser
E	evaporator
G	generator
ext	external
p	pump
w	water

References

[1] OECD/IEA, Technology Roadmap Solar Heating and Cooling, International Energy Agency, 2012.

[2] N. Kalkan, E.A. Young, A. Celiktas, Solar thermal air conditioning technology reducing the footprint of solar thermal air conditioning, Renew. Sustain. Energy Rev. 16 (2012) 6352-6383.

[3] B. Choudhury, P. K. Chatterjee, J. P. Sarkar, Review paper on solar-powered air-conditioning through adsorption route. Renew. Sustain. Energy Rev. 14 (2010) 2189-2195.

[4] M. Izquierdo, R. Lizarte, J. D. Marcos, G. Gutiérrez. Air conditioning using an air-cooled single effect lithium bromide absorption chiller: Results of a trial conducted in Madrid in August 2005. Applied Thermal Engineering 28 (2008) 1074-1081.

[5] A. González-Gil, M. Izquierdo, J. D. Marcos, E. Palacios. Experimental evaluation of a direct air-cooled lithium bromide-water absorption prototype for solar air conditioning. Applied Thermal Engineering 31 (2011) 3358-3368.

[6] J. F. Chen, Y. J. Dai, R. Z. Wang. Experimental and analytical study on an air-cooled single effect LiBr-H2O absorption chiller driven by evacuated glass tube solar collector for cooling application in residential buildings. Solar Energy 151 (2017) 110-118.

[7] U. Jakob, U. Eicker, D. Schneider, A. H. Taki, M. J. Cook. Simulation and experimental investigation into diffusion absorption cooling machines for air-conditioning applications. Applied Thermal Engineering 28 (2008) 1138-1150.

[8] J. Cerezo, M. Bourouis, M. Vallés, A. Coronas, R. Best. Experimental study of an ammonia-water bubble absorber using a plate heat exchanger for absorption refrigeration machines. Applied Thermal Engineering 29 (2009) 1005-1011.

[9] Q. Ma, L. Luo, R. Z. Wang, Z. Z. Xia, P. Lin, B. Souyri. Performance analysis and validation on transportation of heat energy over long distance by ammonia-water absorption cycle. Int. J. of Energy Research 34 (2010) 839-847.

[10] L. B. Le, N. Galanis, J. Millette. Experimental study of an ammonia-water absorption chiller. Int. J. of Refrigeration 35 (2012) 2275-2286.

[11] F. Boudéhenn, H. Demasles, J. Wyttenbach, X. Jobard, D. Chèze, P. Papillon. Development of a 5 kW cooling capacity ammonia-water absorption chiller for solar cooling applications. Energy Procedia 30 (2012) 35-43.

[12] S. A. M. Said, K. Spindler, M. A. El-Shaarawi, M. U. Siddiqui, F. Schmid, B. Bierling, M. M. A. Khan. Design, construction and operation of a solar powered ammonia-water absorption refrigeration system in Saudi Arabia. Int. J. of Refrigeration 62 (2016) 222-231.

[13] S. U. Llamas, J. V. Herrera, R. Cuevas, V. H. Gómez, O. García-Valladares. J. Cerezo and R. Best. Development of a small capacity ammonia-lithium nitrate absorption refrigeration system. 2nd Int. Conference on Solar Air-Conditioning, Tarragona, Spain (2007) pp. 470-475.

[14] S. U. Llamas, R. Cuevas, R. Best, and V. H. Gómez. Experimental results of a direct air-cooled ammonia-lithium nitrate absorption refrigeration system. Applied Thermal Engineering 67 (2014) 362-369.

[15] J. F. Wang, G. C. Gao and G. M. Chen. An improved absorption refrigeration cycle driven by unsteady thermal sources below 100 °C. Int. J. of Energy Research 24 (2000) 633-640.

[16] J. A. Hernández-Magallanes, L .A. Domínguez-Inzunza, G. Gutiérrez-Urueta, P. Soto. C. Jiménez and W. Rivera. Experimental assessment of an absorption cooling system operating with the ammonia/lithium nitrate mixture. Energy 78 (2014) 685-692.

[17] L. A. Domínguez-Inzunza, J. A. Hernández-Magallanes, P. Soto, C. Jiménez, G. Gutiérrez-Urueta, G., W. Rivera. Experimental assessment of an absorption cooling system utilizing a falling film absorber and generator. Applied Thermal Engineering 103 (2016) 1105-1111.

[18] R. Winston, L. Jiang, B. Widyolar. Performance of a 23KW solar thermal cooling system employing a double effect absorption chiller and thermodynamically efficient non-tracking concentrators. Energy Procedia 48 (2014) 1036-1046.

[19] P. Soto, L. A. Domínguez-Inzunza, W. Rivera. Preliminary assessment of a solar absorption air conditioning pilot plant. Case Studies in Thermal Engineering 12 (2018) 672-676.

[20] J. C. Jiménez-García, W. Rivera. Parametric analysis on the performance of an experimental ammonia/lithium nitrate absorption cooling system, Int. J. of Energy Research 42 (2018) 4402-4416.

[21] W. Rivera, G. Moreno-Quintanar, C. O. Rivera, R. Best, and F. Martínez. Evaluation of a solar intermittent refrigeration system for ice production operating with ammonia/lithium nitrate. Solar Energy 85 (2011) 38-45.

[22] G. Moreno-Quintanar, W. Rivera, and R. Best. Comparison of the experimental evaluation of a solar intermittent refrigeration system for ice production operating with the mixtures NH_3-$LiNO_3$ and NH_3-$LiNO_3$-H_2O. Renewable Energy 38 (2012) 62-68.

[23] S. Du, R. Z. Wang, P. Lin, Z. Z. Xu, Q. W. Pan, S. C. Xu. Experimental studies on an air-cooled two-stage NH_3-H_2O solar absorption air-conditioning prototype. Energy 45 (2012) 581-587.

[24] R. Lizarte, M. Izquierdo, J. D. Marcos, E. Palacios. Experimental comparison of two solar-driven air-cooled LiBr/H2O absorption chillers: Indirect versus direct air-cooled system. Energy and Buildings 61 (2013) 323-334.

[25] C. P. Jawahar, R. Saravanan. Experimental studies on air-cooled NH_3-H_2O based modified GAX absorption cooling system. Int. J. of Refrigeration 34 (2011) 658-666.

[26] M. Zamora, M. Bourouis, A. Coronas and M. Vallès. Pre-industrial development and experimental characterization of new air-cooled and water-cooled ammonia/lithium nitrate absorption chillers. Int. J. of Refrigeration 45 (2014) 189-197.

[27] M. Zamora, M. Bourouis, A. Coronas and M. Vallès. Part-load characteristics of a new ammonia/lithium nitrate absorption chiller. Int. J. of Refrigeration 56 (2015) 46-51.

[28] M. Aprile, T. Toppi, M. Guerra, M. Motta. Experimental and numerical analysis of an air-cooled double-lift NH_3-H_2O absorption refrigeration system. Int. J. of Refrigeration 50 (2015) 57-68.

[29] D. Cai, J. Jiang, G. He, K. Li, L. Niu, R. Xiao. Experimental evaluation on thermal performance of an air-cooled absorption refrigeration cycle with NH_3-$LiNO_3$ and NH_3-NaSCN refrigerant solutions. Energy Conversion and Management 120 (2016) 32-43.

[30] A. Goyal, M. A. Staedter, D. C. Hoysall, M. J. Ponkala, S. Garimella. Experimental evaluation of a small-capacity, waste-heat driven ammonia-water absorption chiller. Int. J. of Refrigeration 79 (2017) 89-100.

[31] P. Soto, W. Rivera. Experimental assessment of an air-cooled absorption cooling system. Applied Thermal Engineering 155 (2019) 147-156.

[32] S. P. Verma, L. Díaz-González, J. A. Péerez-Garza, and M. Rosales-Rivera. Quality control in geochemistry from a comparison of four central tendency and five dispersion estimators and example of a geochemical reference material. Arabian Journal of Geosciences 9 (2016) 740-749.